

9B.6 ANALYSIS OF MCV TORNADOES THROUGH STORM-SCALE DATA ASSIMILATION AND SIMULATIONS

Alexander D. Schenkman*¹, Ming Xue^{1,2}, Alan Shapiro^{1,2}, Keith Brewster¹, and Jidong Gao¹

¹*School Of Meteorology, University of Oklahoma, Norman, OK*

²*Center for Analysis and Prediction of Storms, Norman, OK*

1. EVENT DESCRIPTION

On 9 May 2007, several brief tornadoes struck parts of southwest and central Oklahoma. The tornadoes were caused by a strong mesoscale convective vortex (MCV; e.g., Menard and Fritsch 1989) that moved through the region. The first tornado caused EF-1 damage in Grady County, near Minco, OK. Another weak tornado produced EF-0 damage near Union City, OK, in Canadian County. The most destructive tornado, a high-end EF-1, hit El Reno, OK causing an estimated three million U.S. dollars in damage. Two brief EF-1 tornadoes were reported shortly after 0500 UTC 9 May 2007 near Piedmont, OK.

On 4 May 2007, a shortwave trough associated with a 150-kt jet streak propagated southward along the west coast of the United States. A downstream ridge in the Mississippi Valley, and a high-over-low blocking pattern aloft along the east coast of the US prevented the west coast shortwave trough from moving eastward. As a result, by 0000 UTC 7 May 2007, a high-amplitude longwave trough developed in the southwest US. Several shortwave troughs moved through the longwave trough into the Southern and Central Plains. The shortwave troughs resulted in a series of mesoscale convective systems (MCSs) that moved through the southern plains during the period 7-10 May 2007.

One of these MCSs developed on the morning of 8 May 2007 in far eastern portions of New Mexico in an area of upslope flow and moisture advection. Upper-level divergence associated with a shortwave trough ejecting from the longwave trough in the southwestern US aided in this thunderstorm development. The thunderstorm complex grew in areal extent and was located from southwest Oklahoma south to near Del Rio, TX, at 0000 UTC 9 May 2007. The Texas portion of the MCS began to dissipate shortly after 0000 UTC, while new supercell-like development in southwest Oklahoma allowed the northern portion of the MCS to persist until around 0700 UTC.

At approximately 2200 UTC 8 May 2007, a MCV developed in the northern portion of the thunderstorm complex in the vicinity of Wichita Falls, TX. This MCV strengthened and contracted while moving north-northeast into southwest Oklahoma. A supercell in Comanche County, OK, was absorbed by the MCV around 0200 UTC 9 May 2007. The absorbed supercell led to a rapid intensification of the MCV circulation evident in both radar reflectivity and Oklahoma Mesonet (Brock et al. 1995) 10m wind observations (Fig. 1). Additionally, the absorption of the supercell by the MCV caused the supercell to deviate significantly from the mean storm motion. The supercell and other convective elements, which were originally moving northeast, moved in a cyclonic fashion around the center of the MCV. This deviant storm motion significantly enhanced the storm-relative environmental helicity (SREH; e.g., Davies-Jones et al. 1990), which was not very impressive on the KOUN 0000 UTC sounding. Enhancement of SREH combined with vorticity stretching by convective updrafts associated with the MCV created an environment conducive for tornadogenesis (Davies-Jones et al. 2001).

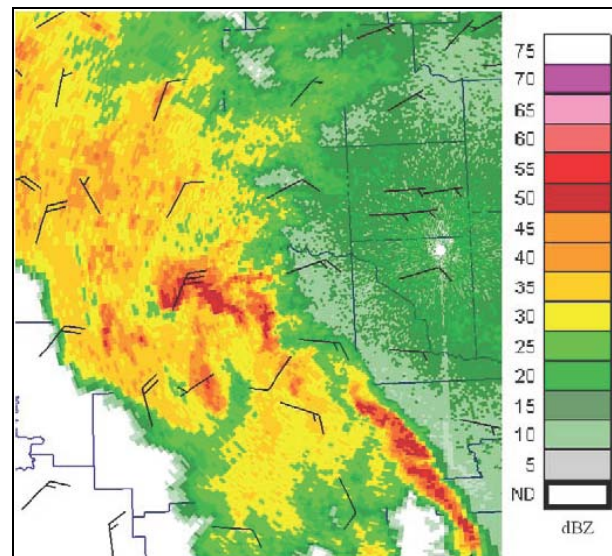


Fig. 1. Reflectivity factor (dBZ) from KTLX from 9 May 2007 at 0305 UTC overlaid with surface winds (kts) from the Oklahoma Mesonet.

* Corresponding Author Address: Alex Schenkman, 120 David L. Boren Blvd., National Weather Center Suite 5357, Norman OK, 73072 Email: alex3238@ou.edu

In addition to the impact of deviant motion, an area of strong horizontal wind shear was also important for the development of tornadoes. Radial velocity observations from the Terminal Doppler Weather Radar (TDWR; Turnbull et al. 1989) at Will Rogers World Airport reveal a strong area of shear and convergence associated with the MCV (Fig. 2). TDWR data suggest that all of the tornadoes associated with the MCV developed initially in this convergent shear zone. The vortices rotated around the northeast portion of the MCV, most likely strengthening due to stretching of vorticity.



Fig. 2. Radial velocity (in knots) observed at 0442 UTC 9 May 2007 by the TDWR in Oklahoma City.

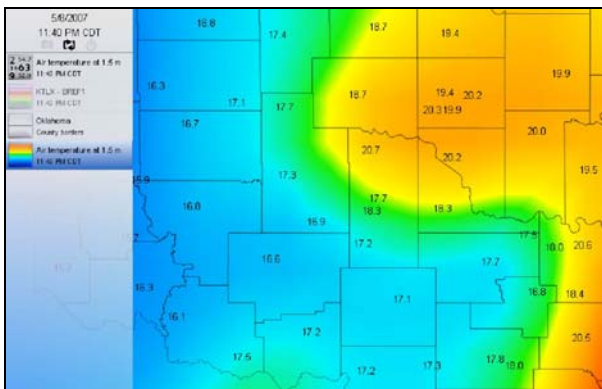


Fig. 3. Temperature field (in C°) at 0440 UTC 9 May from the Oklahoma Mesonet.

From temperature data on the Oklahoma Mesonet (Fig. 3), it can be inferred that the persistent shear zone likely resulted from the MCV circulation and its interaction with the low-level cold pool. Specifically, the MCV advected the cold pool around its southern side, while to its north the air remained relatively warm. As a result, an area of baroclinically generated vorticity (a shear zone) developed. Unfortunately, Oklahoma Mesonet data are too coarse to fully resolve the wind and thermodynamic structure of this shear zone. By 0600 UTC, the shear zone dissipated as a quasi-occlusion process took place with the cold pool advecting all the way around the MCV. Additionally,

the cold pool's relative strength weakened as it moved into cooler air in northern Oklahoma. At 0730 UTC the MCV had completely dissipated, leaving behind a steadily shrinking area of light rain in northeast Oklahoma.

2. SIMULATIONS

The Advanced Regional Prediction System (ARPS; e.g. Xue et al. 2003) model was used to simulate the tornadic convective system. A series of analyses (assimilation window) that assimilated remote sensing and in-situ observations were performed using the ARPS 3DVAR (Gao et al. 2004). Specifically, conventional data (RAOBS, ASOS surface observations etc.), Oklahoma Mesonet data, and radar observations from WSR-88D and the center for Collaborative and Adaptive Sensing of the Atmosphere (CASA; McLaughlin et al 2005) IP1 radar test bed are used.

Data assimilation and forecast experiments are conducted on two one-way nested grids that have 2 km and 400 m grid (hereafter, LR and HR) spacings (Fig. 4). Data assimilation is performed on both grids. On the LR grid, data are assimilated every 5 minutes over a 1 hour assimilation window. On the HR grid, data are assimilated every 5 minutes for assimilation window lengths of between 40 and 80 minutes. A wide variety of experiments were conducted with variable data sets. Further details of the assimilation procedure and model physics configuration can be found in Schenkman (2008).

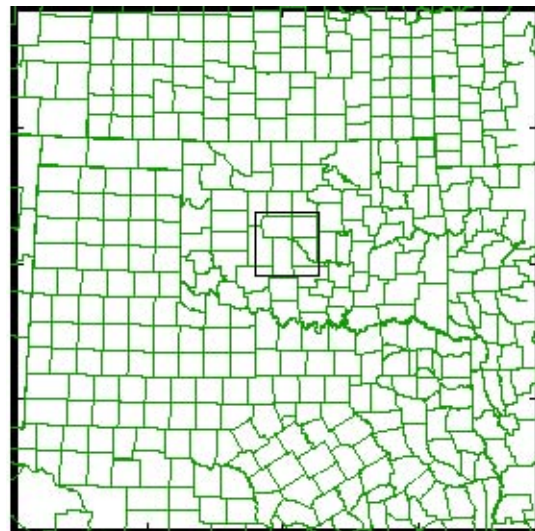


Fig. 4. Map of the outer domain. The black square outlines the inner domain.

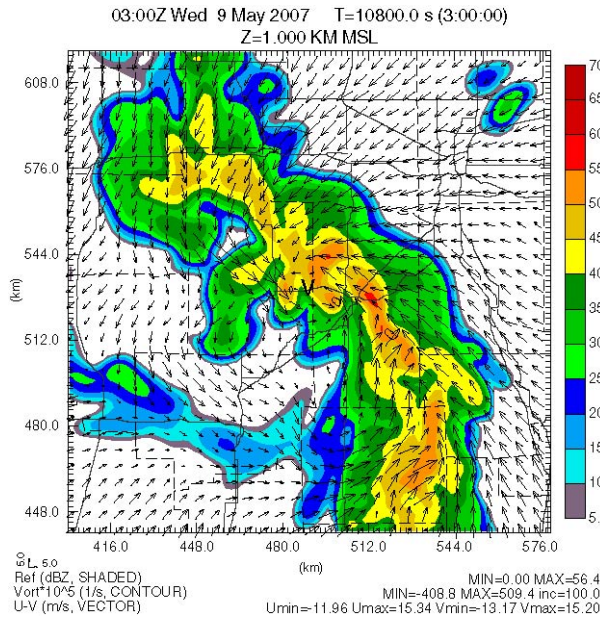


Fig. 5. Forecast from LR experiment at 0300 UTC at 1.0 km MSL. Reflectivity (dBZ) is shaded, contours vorticity ($10^5 s^{-1}$), vectors are horizontal wind (in ms^{-1}).

In this paper[†], we focus on two experiments: one on the LR grid and one on the HR grid. Our chosen LR grid experiment simulates the 9 May 2007 event with great accuracy and is examined to further explore the dynamics of the MCV. The chosen HR grid experiment features an 80 minute assimilation window. The tornado-like vortices (TLVs) that develop within the HR grid experiment are fairly representative of the structure of the TLVs in the other experiments described in Schenkman (2008). For our purposes, a TLV is defined as a circulation below a height of 2km with maximum vertical vorticity exceeding $0.05 s^{-1}$ persisting for more than 5 minutes.

2.1 2km Resolution Simulation

The LR experiment forecast period begins at 0200 UTC with a large MCS over southwest Oklahoma and northwest Texas. The strongest convection (based on reflectivity factor) is present in southwest Oklahoma in the northern portion of the MCS (not shown). By 0300 UTC, most of the convection within TX has dissipated while a weak vortex has developed in the northern portions of the convection in SW OK (Fig. 5). The vortex appears to be generated within a shear zone between strong west winds (rear-inflow) behind the gust front, southeasterly flow in advance of the gust

[†] It should be noted that the present paper is an extension of Schenkman et al. (2008).

front, and an area of enhanced northwest flow moving south immediately to the west of the vortex.

The weak vortex strengthens through 0445 UTC as it moves NNE through west-central OK (Fig. 6). Vorticity stretching within the persistent updraft of a strong convective cell co-located with the vortex appears to be the primary mechanism for the strengthening trend of the vortex (Fig. 7). Thus, vortex maintenance and intensification is similar to a book-end/mesocyclone-like vortex.

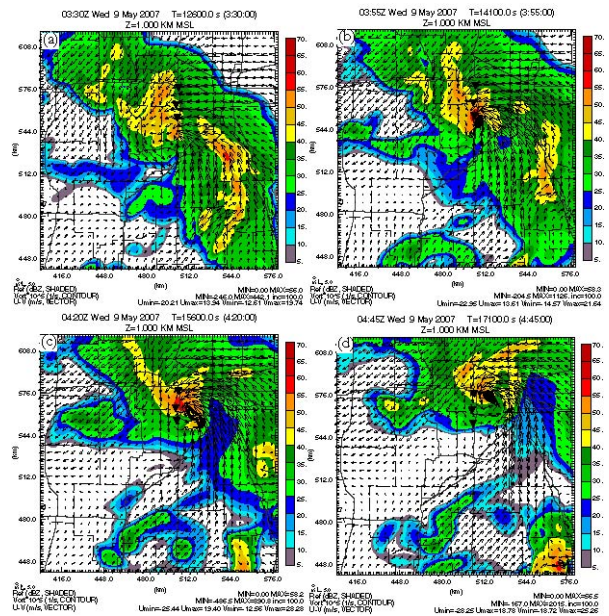


Fig. 6. As Fig. 5. except at (a) 0330 UTC, (b) 0355 UTC, (c) 0420 UTC, (d) 0445 UTC.

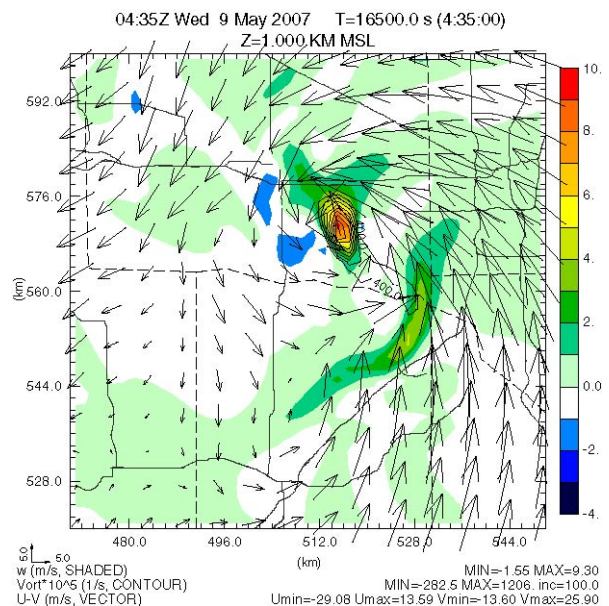


Fig. 7. Forecast vertical velocity (shaded, in ms^{-1}) and vorticity (contoured, $10^5 s^{-1}$) and wind vectors (ms^{-1}) at 1.0 km MSL at 0435 UTC.

As the vortex moves NNE, it passes within 10 km of the reported locations of the Minco, Union City, and El Reno (i.e. in comparison to the black triangles in Fig. 6). In fact, the vortex has two peaks in intensity (as measured by vorticity at 1.0 km ASL): one around 0400 UTC as it passes near Minco and Union City, and a second stronger peak at 0445 UTC near El Reno (not shown). At the end of the forecast period (0500 UTC), the vortex weakens but is still present to the east of El Reno.

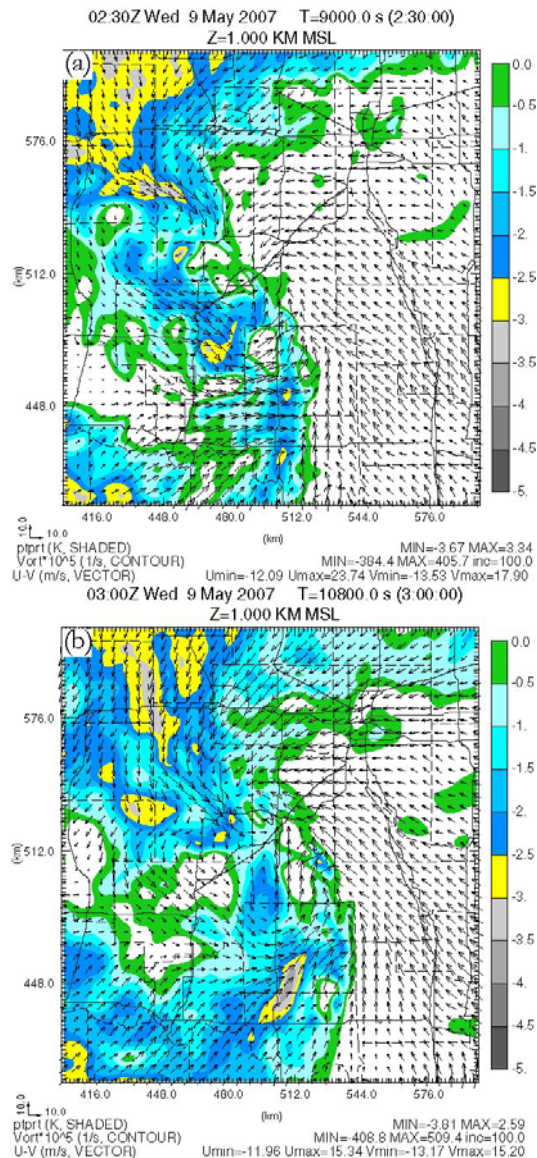


Fig. 8. LR forecast cold pool (shaded in K) and wind vector (ms^{-1}) at (a) 0230 UTC and (b) 0300 UTC.

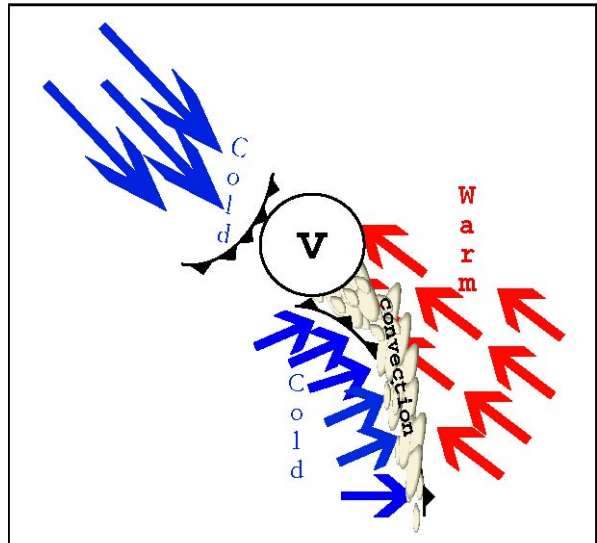


Fig. 9. Schematic of vortex development in the LR experiments. The 'v' represent the vortex location.

Examination of the low-level cold pool helps to further explain the generation of the vortex. Figure 8a shows that at 0230 UTC there are two distinct cold pools associated with the portion of the MCS in west-central OK. One part of the cold pool is co-located with the convective line and another is removed to the northwest of the convection. As the simulation proceeds the cold pool co-located with the convection moves slowly to the east and northeast while the cold pool to the northwest of the convection surges to the southeast (Fig. 8b). The vortex forms as the two cold pools merge.

After the vortex forms, it advects the cold pool (predominantly located to its south) to the north and west. The vortex (and related updraft) reaches its peak strength shortly before it occludes. After occlusion, the vortex and associated updraft gradually weaken. Figure 9 provides a schematic that illustrates the vortex formation.

2.2 400m Resolution Simulation

At the beginning of the 400m resolution simulation (0220 UTC 9 May 2007), a line of convection is present in the southwest corner of the domain with stratiform rain in the northwest portion of the domain. The convection moves to the northeast, and by 0300 UTC is located in a line from southeast Grady County northwest to northern Caddo County (not shown). The northern portion of the line is made up of numerous small convective cells, while the southern portion of the line is fairly continuous. A MCV is present within the northern portion of the convective line.

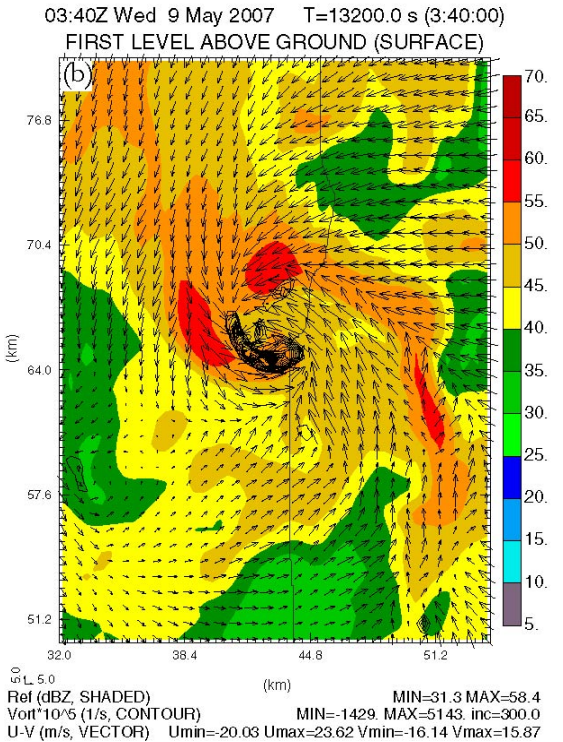
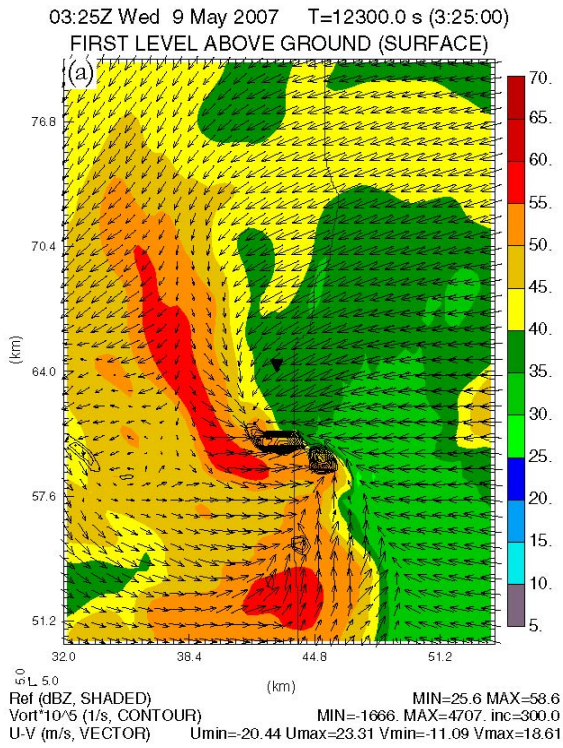


Fig. 10. Forecast Minco TLV at (a) 0325 UTC and (b) 0340 UTC. Fields are as in Fig. 5.

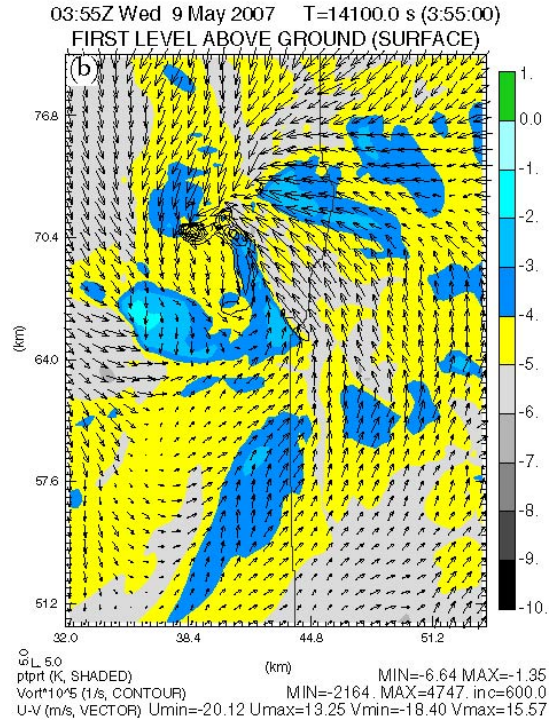
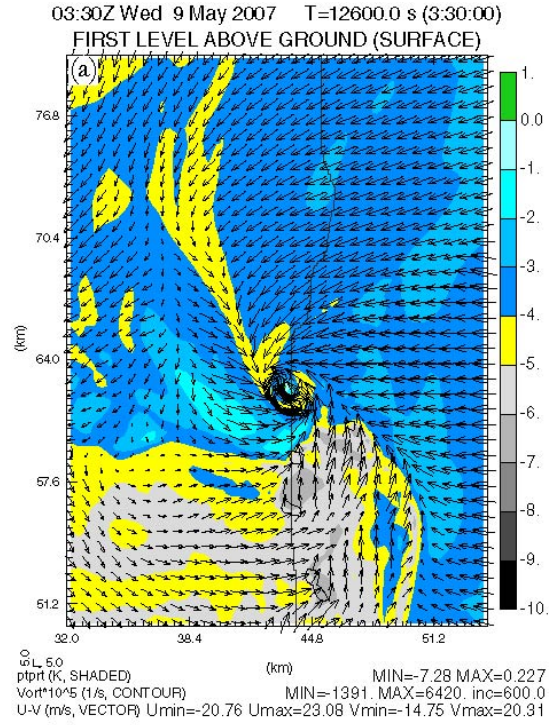


Fig. 11. HR forecasted near-surface cold pool (shaded, in K), wind vectors (ms^{-1}), and vorticity ($10^5 s^{-1}$) at (a) 0330 UTC and (b) 0355 UTC.

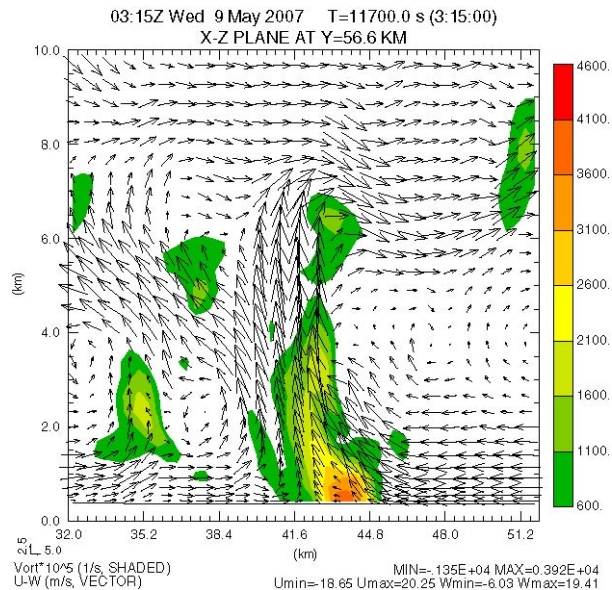


Fig. 12. Vertical x-section through developing Minco TLV at 0315 UTC. Vertical vorticity is shaded (in 10^5 s^{-1}) vectors are wind in $x-z$ plane (in ms^{-1}).

Vertical cross sections reveal the TLV develops within a deep updraft that extends from low-levels up to about 8 km (Fig. 12).

The sub storm-scale features of the simulation become significant around 0310 UTC as a low-level circulation develops south of Minco. This circulation moves to the north while strengthening rapidly, reaching tornado-like vortex (TLV) criteria by 0325 UTC about 5 km south of Minco (Fig. 10a). (Here a TLV is defined as a circulation below a height of 2 km with maximum vertical vorticity exceeding 0.05 s^{-1} persisting for more than 5 minutes) At 0340 UTC, the TLV tracks within 1 km of the reported Minco tornado location with a maximum vorticity value $\sim 0.14 \text{ s}^{-1}$ (Fig. 10b). As the TLV continues to move north, it slowly weakens. Following the dissipation of the TLV, a number of transient strong vorticity centers develop. It is difficult to determine if these circulations are TLVs or just transient areas of shear because they are very short-lived. However, one brief TLV does form near Union City around 0405 UTC. Eventually, another less transient TLV develops less than 5 km to the northwest of El Reno at 0445 UTC. This TLV moves northwest and weakens by the end of the simulation.

All three TLVs appear to be associated with strong convection and a strong convergence/shear zone in the center and western half of the MCV. We can examine the cold pool in order to find the origin of this convergence/shear zone. As in the LR experiment, the forecast begins with two separate cold pools; a strong convectively generated cold pool with a north-south oriented gust front in the southwest portion of the domain, and a weaker stratiform precipitation generated

cold pool with a southwest-northeast oriented gust front in the northwest portion of the domain. In the first 30 minutes of the forecast, the weaker cold pool surges to the southeast, while the convective cold pool moves slowly to the east. By 0300 UTC, the two cold pools merge in eastern Caddo County forming a new gust front which surges to the east. The Minco TLV develops on the northern portion of this gust front and rapidly strengthens. The flow associated with the TLV advects the cold surge to the north and west and sets up a persistent area of convergence between the northwest flow on the west side of the MCV and southeast flow within the cold surge.

To the east of this convergence zone, a shear zone is present between the southeast winds in the cold surge and northeast winds due to the MCV circulation. Vorticity is generated in this shear zone and is advected to the west into the convergence zone, where it is stretched by convection. This process is highly nonlinear, as each transient vortex and TLV affect the MCV circulation.

3. TLV ANALYSIS

A closer analysis of the forecast, specifically the TLVs, reveals a relatively warm semi-annular downdraft is present surrounding the TLVs. The downdrafts appear to be a result of the TLV circulation, as the downdrafts typically develop several minutes after the TLV. We consider the TLV that passed near Minco to examine the evolution and dynamics behind the warm downdrafts in more detail. The TLV initially forms on a strong gust front in an area of strong convergence at 0310 UTC. To the west of the TLV the air is relatively cold, while to its east the temperature is close to the base state. As the TLV strengthens, the temperature to its south and immediately to its north warms several K. By 0330 UTC, the TLV is surrounded by relatively warm air to its west and northeast, but has a cold perturbation at its center (Fig. 11a). The TLV weakens after 0345 UTC, and the warm air rapidly cools to the temperature of the cold pool by 0355 UTC (Fig. 11b).

The TLV forms just behind the gust front that is responsible for initiating this updraft. By 0320 UTC, an updraft is present within and above the TLV, but a shallow downdraft has developed to the east and west of the TLV. The downdraft is confined to the lowest 4 km, and above it the updraft continues. The downdraft to the west of the TLV reaches the ground and diverges with some air flowing to the west, and the rest flowing east into the TLV. The TLV continues to strengthen, and by 0328 UTC an 8-10 mb negative pressure perturbation has developed in the lowest 2 km of the atmosphere near the center of the TLV (Fig. 13). The western half of the pressure drop features a strong

updraft, while the eastern half has a strong downdraft.

Another downdraft is located approximately 3km to the southwest. By 0335 UTC, the two separate downdrafts merge to the south of the TLV (Fig. 14a). There are still two separate minima in the vertical velocity field. One minimum is just to the north of the TLV, while the second is nearly 5km to the west. The updraft also has two discernible maxima. A vertical velocity maximum is present immediately to the south and west of the TLV, with another maximum, in a configuration resembling a flanking line, to the east and southeast of the TLV.

The two downdraft maxima appear to have different origins. The downdraft to the west is likely associated with precipitation wrapping around the circulation. This leads to downward vertical velocity caused by precipitation. The downdraft likely overshoots its equilibrium and warms through compression. The downdraft maximum immediately to the north of the TLV appears to be a direct result of the strong pressure perturbation associated with the TLV. Figure 14a shows substantially less q_r associated with this downdraft than with the downdraft to the west of the TLV, further demonstrating that this downdraft is caused by the strong pressure perturbation and not water-loading.

The downdraft structure present in our simulation is remarkably similar to the occlusion/rear flank downdraft (RFD) structure observed and simulated in supercells (e.g. Brandes 1978; Klemp and Rotunno 1983; Wicker and Wilhemson 1995). In these studies the

occlusion downdraft formed within the broader RFD as a result of the pressure perturbation within the tornado. The updraft/downdraft configuration shown in Fig. 14b (from Wicker and Wilhemson 1995) is very similar to that shown in Fig. 14a.

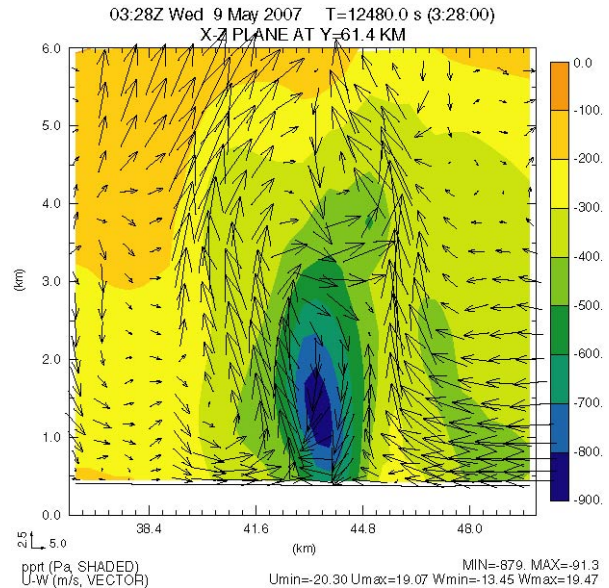


Fig. 13. Vertical x-section through Minco TLV at 0328 UTC. Perturbation pressure is shaded (Pa) and vectors are wind in the x-z plane (in ms^{-1}).

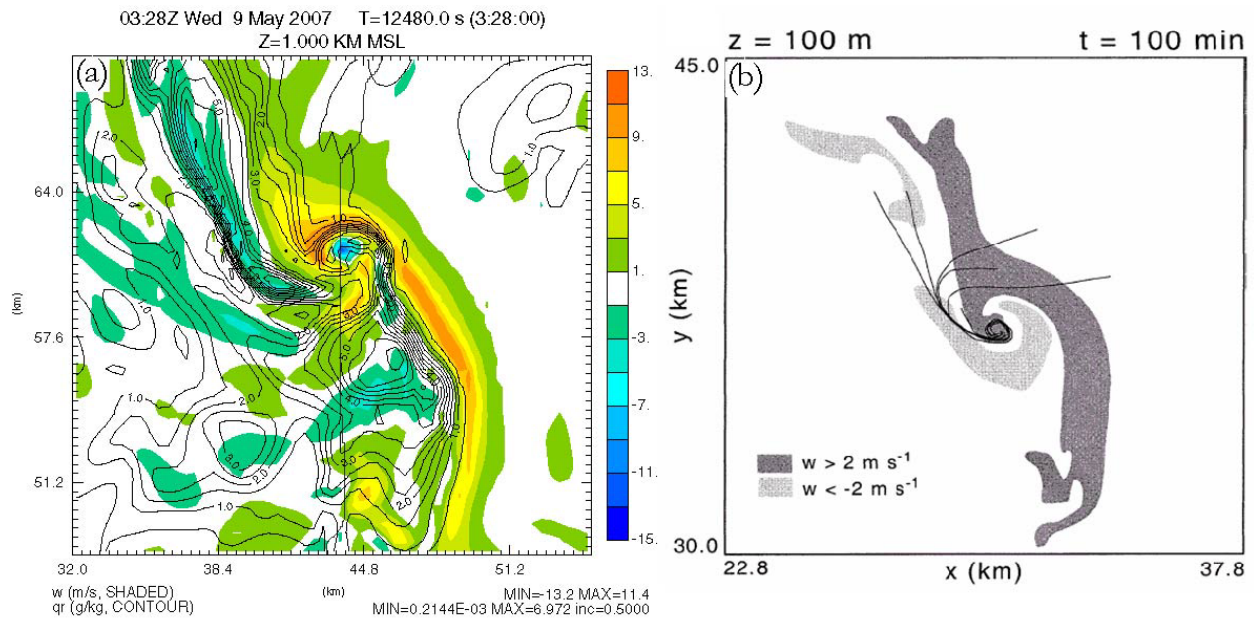


Fig. 14. Comparison between the present simulation and that of supercell tornadogenesis by Wicker and Wilhemson (1995), adapted by Markowski (2002). (a) The near-surface vertical velocity field in m s^{-1} (colored) and the horizontal velocity vectors from the simulation at 0332 UTC. (b) Near-surface vertical velocity fields with dark shading indicating updrafts and light shading indicating downdrafts. Tornado parcel trajectories are also shown.

In addition, as in our study, the occlusion downdraft was observed to begin at low-levels before growing in vertical extent with time. The similarities between the occlusion downdraft and the downdrafts associated with the TLV suggest the thunderstorms that develop TLVs briefly take on supercellular characteristics. This is somewhat unexpected because the storms associated with the TLVs are not within an environment typically associated with supercells. Additionally, the aforementioned similarities lend credence to the idea that the TLVs are realistic representations of tornadoes within the model.

4. SUMMARY AND FUTURE WORK

In this study, we have presented a detailed analysis of the west-central Oklahoma 9 May 2007 tornadic MCV. The genesis, maintenance, and intensification of the MCV and related tornado vortices have been explored through observations and high-resolution simulations. Additionally, the high-resolution simulations reveal supercell-like features in the convective system. Specifically, the development of simulated tornado-like vortices show striking similarities to well-established conceptual models of supercell tornadogenesis.

In addition to providing insight into the processes behind the 9 May 2007 convective system, numerical simulations also showed great accuracy in their portrayal of the system's evolution. Highly accurate forecasts of TLVs at up to 2 h in advance, lead to a host of questions about predictability. Namely, how much of the forecast accuracy is coincidental? Is this degree of accuracy reproducible when applied to other severe convective storm cases? Future work will focus on additional sensitivity and predictability experiments in attempt to answer these important questions.

Acknowledgement: This work was primarily supported by NSF grant EEC-031347, through Engineering Research Center (ERC) for Collaborative Adaptive Sensing of the Atmosphere (CASA).

REFERENCES

- Brandes, E. A., 1978: Mesocyclone evolution and tornadogenesis: Some observations. *Mon. Wea. Rev.*, **106**, 995–1011.
- Brock, F. V., K. C. Crawford, R. L. Elliott, G. W. Cuperus, S. J. Stadler, H. L. Johnson, and M. D. Eilts, 1995: The Oklahoma Mesonet: A technical overview. *J. Atmos. Oceanic Technol.*, **12**, 5–19.
- Davies-Jones, R., D. Burgess, and M. Foster, 1990: Test of helicity as a tornado forecast parameter. Preprints, 16th Conf. Severe Local Storms, Kananaskis Park, AB, Canada, Amer. Meteor. Soc., 588–592.
- , R. J. Trapp, and H. B. Bluestein, 2001: Tornadoes and tornadic storms. *Severe Convective Storms. Meteor. Monogr.*, No. 50, Amer. Meteor. Soc., 167–221.
- Gao, J., M. Xue, K. Brewster, and K. K. Droegemeier, 2004: A three-dimensional variational data analysis method with recursive filter for Doppler radars. *J. Atmos. Oceanic Technol.*, **21**, 457–469.
- Klemp, J. B., and R. Rotunno, 1983: A study of the tornadic region within a supercell thunderstorm. *J. Atmos. Sci.*, **40**, 359–377.
- Markowski, P.M., 2002: Hook echoes and rear-flank downdrafts: A review. *Mon. Wea. Rev.*, **130**, 852–876.
- McLaughlin, D.J., V. Chandrasekar, K. Droegemeier, S. Frasier, J. Kurose, F. Junyent, B. Philips, S. Cruz-Pol, and J. Colom, 2005: Distributed Collaborative Adaptive Sensing (DCAS) for Improved Detection, Understanding, and Prediction of Atmospheric Hazards. 9th Symp. Integrated Obs. Assim. Systems - Atmos. Oceans, Land Surface (IOASAOLS), Amer. Meteor. Soc., San Diego, CA.
- Menard, R. D., and J. M. Fritsch, 1989: A mesoscale convective complex-generated inertially stable warm core vortex. *Mon. Wea. Rev.*, **117**, 1231–1267.
- Schenkman, A.D., 2008: High resolution assimilation of CASA and WSR-88D for the prediction of a tornadic convective system. M.S. Thesis, University of Oklahoma. [Available from the University of Oklahoma School of Meteorology, 120 David L. Boren Blvd, Norman, OK, USA, 73072].
- , C. M. Shafer, and M. Kumjian, 2008: Multi-platform analysis of a tornadic convective system. Preprints, *ERAD 2008-The Fifth European Conference on Radar in Meteorology and Hydrology*, Helsinki, Finland.
- Turnbull D., J. McCarthy, J. Evans, and D. Zrnich, 1989: The FAA Terminal Doppler Weather Radar (TDWR) program. Preprints, *Third Int. Conf. on Aviation Weather Systems*, Anaheim, CA, Amer. Meteor. Soc., 414–419.
- Wicker, L. J., and R. B. Wilhelmson, 1995: Simulation and analysis of tornado development and decay within a three-dimensional supercell thunderstorm. *J. Atmos. Sci.*, **52**, 2675–2703.
- Xue, M., D.-H. Wang, J.-D. Gao, K. Brewster, and K.K. Droegemeier, 2003: The Advanced Regional Prediction System (ARPS), storm-scale numerical weather prediction and data assimilation. *Meteor. Atmos. Physics*, **82**, 139–170.